JOURNAL OF CATALYSIS 137, 429–436 (1992)

# A Mechanistic Study of the Oxygen Insertion into $MoO_3$ Crystals as Revealed by SIMS and TPSR Techniques

A. GUERRERO-RUÍZ,* J. M. BLANCO,† M. AGUILAR,† I. RODRÍGUEZ-RAMOS,‡ AND J. L. G. FIERRO‡

*Departamento de Química Inorgánica, Facultad de Ciencias, UNED, 28040 Madrid, Spain; †Departamento de Tecnología Electrónica, ETSI, Telecomunicación, UPM, 28040 Madrid, Spain; and ‡Instituto de Catálisis y Petroleoquímica, CSIC, Cantoblanco, UAM, 28049 Madrid, Spain

Received November 25, 1991; revised April 3, 1992

Static secondary ion mass spectroscopy (SIMS) and temperature-programmed surface reaction (TPSR) probes were used to characterize the nature and participation of oxygen species of $MoO_3$ crystals in the selective oxidation of propylene. The SIMS analysis of the oxygen-18-containing fragments of two $MoO_3$ crystals, possessing different exposed crystallographic planes and pretreated under the $^{18}O_2 + C_3H_6$ mixture, allowed monitoring of the directional $^{18}O$ labeling within the crystals. Moreover, the insertion level of oxygen-18 into the acrolein reaction product has been evaluated by mass spectroscopy. TPRS of chemisorbed NO has been used to evaluate the reactivity of surface oxygen ions. From these results a simple model for explaining the observed structure-sensitive partial oxidation of propylene on well-defined $MoO_3$ crystal structures is proposed.


## INTRODUCTION

One of the key questions in the selective oxidations of hydrocarbons on metal oxides is the mechanism of oxygen insertion into the hydrocarbon molecules, resulting in partial oxidation. This step includes both the activation of dioxygen molecule and the further insertion of the resulting oxygen ions into the hydrocarbon molecule or the organic intermediate adsorbed on the catalyst surface. As already advanced in the early fifties (*1*), the latatice oxygen was assumed to be directly involved in the hydrocarbon oxidation.

An elegant experimental confirmation of this mechanism was obtained in the sixties for olefin oxidation using $^{18}O_2$ as an oxidant and monitoring the oxygen distribution in the effluents of the reactor by mass spectrometry. Following this methodology, the pioneer works of Keulks and co-workers (*2–4*) on propylene oxidation demonstrated that the oxygen comes from the lattice oxygen over Bi–Mo oxide catalysts. From further revisions on the subject (*5, 6*) there is no doubt about the relevance of isotopic labeling in elucidating the mechanisms of hydrocarbon oxidations, but it becomes apparent that no direct information on the processes taking place at the catalyst surface can be derived from this technique alone. Thus, there is only little information about the sites involved in dioxygen activation, the reaction route of oxygen ions within the solid, and the directional reactivity of the crystal faces of oxide catalysts. To address these questions, secondary ion mass spectrometry (SIMS) seems, in principle, an interesting technique for monitoring the oxygen evolution within this type of catalyst. The strategy could be to analyze model catalysts, in which specific crystal planes have deliberately been $^{18}O$-labeled during the hydrocarbon oxidation.

Although the SIMS technique has not been widely applied in the characterization of catalysts (*7*), the high surface sensitivity of the static SIMS was exploited by Rodrigo *et al.* (*8*) to reveal the dispersion of molyb-



0021-9517/92 $5.00

dena in supported catalysts, by Takahashi *et al.* (*9*) to probe the local atomic environment of $VO_x$-promoted Ru catalysts used in FT synthesis, and more recently by Meijers *et al.* (*10*) to study the dispersion of $ZrO_2$ in supported catalysts. However, in no case has the SIMS technique been used with the aforementioned aim. $MoO_3$ catalysts seem attractive examples for these studies, since it has recently been demonstrated that oxidation of olefins on $MoO_3$ is structure sensitive (*11, 12*). For propene oxidation, it has been found that combustion occurs on the basal (010) plane while acrylaldehyde is produced on the lateral (100) planes. Also, the allylic species, which are primary intermediates of the reaction, have been found to oxidize to acrylaldehyde more easily on the lateral planes of $MoO_3$ (*13*). This finding is confirmed by oxygen-18 tracer studies which indicated a higher proportion of oxygen-18 in the resulting acrolein, when $MoO_3$ shows a great proportion of lateral faces (*14*). In light of these studies, it seems that dioxygen activation and further oxygen insertion occur on the (100) faces. However, this picture cannot be taken as conclusive, since other authors proposed the (010) face of $MoO_3$ for oxygen insertion (*15*).

It is the aim of the present work to gain further insight into the oxygen incorporation process on $MoO_3$ crystals. This is achieved by monitoring the oxygen-18 insertion both in the oxide by SIMS and in the reaction products of propene and $^{18}O_2$ by mass spectrometry. Finally, the reactivity of the most abundant $MoO_3$ faces is followed by the temperature-programmed surface reaction (TPSR) of chemisorbed NO.

## EXPERIMENTAL

### *Catalysts*

Three different $MoO_3$ samples have been used in this study. The [010]-oriented single crystal with the (010) face largely developed, at least 90% of the total surface, was prepared by evaporation-condensation of $MoO_3$ under an oxygen stream (*16*). $MoO_3$ sheets, with the preferential [100] orientation, were prepared by oxidation of Mo foil at 953 K for 6 h (*17*). This latter sample also shows lateral (lk0) faces as constituents of the dominant (l00) faces. For the experiments of temperature-programmed surface reaction of chemisorbed NO a commercial polycrystalline $MoO_3$ (Merck, reagent grade) sample was also used.

### *Techniques and Procedure*

The SIMS spectra were recorded using a Balzers quadrupole mass analyzer (0–511 amu) assembled on an UHV Leybold system capable of attaining a base vacuum of $10^{-10}$ Torr (1 Torr = 133.33 N $m^{-2}$) and of $3 \times 10^{-9}$ Torr during data acquisition. The secondary positive ions were mass analyzed in the quadrupole mass filter and detected by an electron multiplier. The primary ion beam was $Ar^+$ (hot cathode) of 3 keV energy and the beam current of 5 nA $cm^{-2}$. The diameter of the ion beam was close to 0.2 mm. As the $MoO_3$ samples are essentially insulant, they were neutralized during analysis using a flood gun of less than 0.7 keV energy. The samples used in this study were the $MoO_3$ (010) and $MoO_3$ (100) crystals, the latter prepared by oxidation of molybdenum foil at 953 K. The SIMS spectra were first obtained for air-stabilized samples (aged for more than 2 months under atmospheric conditions after synthesis), then for the same samples after exposure to the reactive mixture ($^{18}O$ + propylene), according to the following procedure. (010)- or [100]-oriented $MoO_3$ crystals were heated at 673 K for 1 h in a quartz reactor under a pressure of $^{16}O_2$. After cooling to room temperature, the samples were outgassed and contacted with a $C_3H_6$ : $^{18}O_2$ = 1 : 2 mixture at a total pressure of 60 Torr. When the samples were heated at a rate of 5 K $min^{-1}$ up to 673 K, maintaining this temperature for 2 h. After cooling to room temperature, they were transferred into the vacuum chamber of the SIMS spectrometer. SIMS analysis was carried out by monitoring essentially the masses of $MoO^+$ fragments for long periods of time. Since the surface is progressively

eroded by $Ar^+$ ions, the SIMS technique coupled with depth profiling is an ideal technique for monitoring oxygen-18 enrichment levels as a function of depth.

The gas phase of catalysts exposed to the reactant $C_3H_6 + {}^{18}O_2$ mixture was analyzed by mass spectrometry using a Balzers QMG-125 mass spectrometer coupled online with the reaction system. Provided a static pretreatment was used and the resulting acrolein can be degraded to $CO_2$ (*18*), the gas-phase analysis was focused on the masses $m/e = 56$ and 58 corresponding to ${}^{16}OC_3H_4$ and ${}^{18}OC_3H_4$, respectively. To follow a possible evolution of ${}^{18}O_2$ incorporation during the reaction, these analyses were extended to different reaction times.

The TPSR of chemisorbed NO was also monitored by mass spectrometry. This study was conducted on [100]-oriented $MoO_3$ and polycrystalline $MoO_3$, the latter being preferable to (010) $MoO_3$ crystals due to its higher specific surface. Prior to NO chemisorption the samples were cleaned by heating under vacuum up to 723 K for 2 h. After cooling to room temperature they were contacted with 40 Torr NO for 1 h and allowed to reach equilibrium. Once the gas phase has been removed, the temperature was increased at a rate of 5 K $min^{-1}$ and desorbed products were analyzed continuously by mass spectrometry. The masses corresponding to NO ($m/e = 30$), $N_2O$ ($m/e = 44$), and $NO_2$ ($m/e = 46$), and some of their secondary lines, mainly were analyzed.

## RESULTS

A large part of this work is concerned with establishing the sites responsible for dioxygen activation and the directions preferred for oxygen migration during selective oxidation of propene on $MoO_3$. This requires indeed a reliable analysis of the solid, not only quantitative but also capable of discriminating between ${}^{16}O$- and ${}^{18}O$-containing fragments. Secondary ion mass spectra of the nonlabeled (010) $MoO_3$ crystal in the region of 90 to 120 amu is given in Fig. 1. In

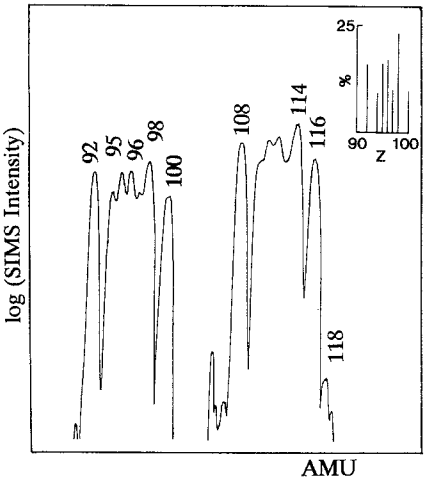


FIG. 1. SIMS spectra of the air-stabilized (010) $MoO_3$ crystals in the amu range corresponding to $MoO^-$ masses. The inset represents the isotope abundances of Mo.

this plethora of peaks, the ones corresponding to $Mo^+$ isotopes (92–100 amu), as well as those relative to $MoO^+$ fragments (108–116 amu), can be distinguished. A similar SIMS pattern has already been recorded for the oriented [100] crystal.

Before embarking on the isotopic labeling study, two salient features of mass spectra must be considered: (i) upon ${}^{18}O$ incorporation into $MoO_3$ a peak at 118 amu due to ${}^{100}MoO{}^{18}O^+$ should be observed; (ii) to establish intensity ratios between ${}^{18}O$-labeled and ${}^{16}O$-nonlabeled $MoO^+$ fragments, peaks at 118 and 108 amu, corresponding to ${}^{100}Mo{}^{18}O^+$ and ${}^{92}Mo{}^{16}O^+$ ions, respectively, must be considered. Note that selection of mass 108 for $MoO^+$ in point (ii) is a good internal standard since it contains the lower ${}^{92}Mo$ isotope and ${}^{16}O$. Figure 2 shows the secondary ion mass spectrum of a $MoO_3$ sample used in the oxidation of propene with ${}^{18}O_2$. By comparing this spectrum with that of the fresh $MoO_3$ sample (Fig. 1) it becomes clear that the peak at 118 amu increases to a great extent, which confirms that oxygen-18 is incorporated into the solid in the course of the reaction.

Another important aspect is the rate of

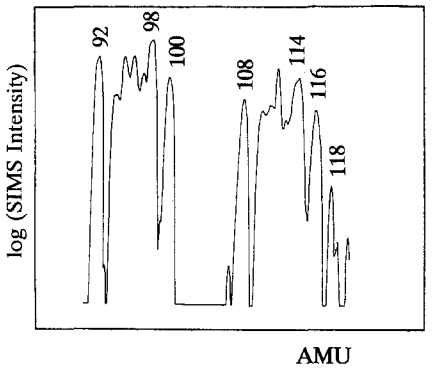


FIG. 2. SIMS spectra of the (010) $MoO_3$ crystals previously exposed to a $^{18}O_2 : C_3H_6 = 2 : 1$ (molar) mixture at 673 K for 2 h.

lattice oxygen migration through the solid and its preferential diffusion in a given direction. As stated above, depth profiling combined with SIMS analysis of $MoO^+$ fragments for different crystal orientations may fulfil these expectations. At this point, it also must be noted that the analysis of (010) $MoO_3$ crystals will proceed along the [010] direction while the [100] direction will be followed when $MoO_3$ crystals prepared by oxidation of Mo foil are analyzed. Figure 3 shows intensity changes of $Mo^{16}O^+$ and $Mo^{18}O^+$ fragments of both samples for periods up to 4 h. It can be observed in Fig. 3a that the (010) $MoO_3$ face leads to a larger decrease of the $Mo^{18}O^+$ (amu = 118) signal than of the $Mo^{16}O^+$ (amu = 108) counterpart. A similar behavior is observed for the [100]-oriented $MoO_3$ crystal (Fig. 3b), which also possesses lateral faces on the surface. As a consequence, even if the decrease of the latter (amu = 108) signal may be merely due to experimental artifact, the larger decrease of the former (amu = 118) signal cannot be explained in a similar manner. Accordingly, these results indicate that diffusion of $^{18}O$-atoms within the $MoO_3$ crystal is a slow process, at least under the experimental conditions used in this study.

To monitor better the tendencies already shown in Fig. 3, the logarithmic SIMS intensity ratio $Mo^{18}O^+/Mo^{16}O^+$ has been plotted

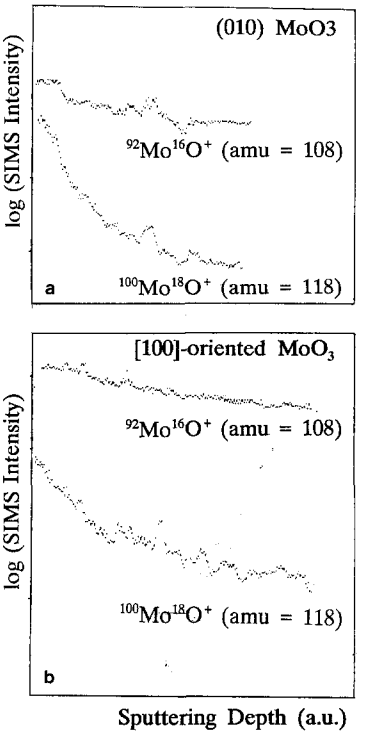


FIG. 3. Dependence of the SIMS intensities on the sputtering depths for $^{92}Mo^{16}O^+$ (amu = 108) and $^{100}Mo^{18}O^+$ (amu = 118) fragments in (010)-oriented (a) and [100]-oriented (b) $MoO_3$ crystals.

in Fig. 4 as a function of the sputtering depth for the two $MoO_3$ samples. It can be noted readily that the (010) $MoO_3$ leads to a larger decrease of this ratio (from 1.0 to 0.04), while its absolute decrease is less marked

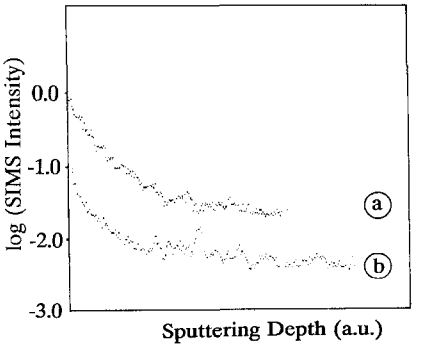


FIG. 4. SIMS relative intensity ratios $^{100}Mo^{18}O^+/^{92}Mo^{16}O^+$ as a function of the sputtering depth for the (010)-oriented (a) and [100]-oriented (b) $MoO_3$ crystals.

TABLE 1

Extent of Oxygen-18 Incorporation into the Acrolein

| Sample | Reaction time (h) | $C_3H_5{}^{18}O/C_3H_5{}^{16}O$ |
|---|---|---|
| (010) $MoO_3$ | 1 | 2.2 ± 0.2 |
| | 2 | 2.7 ± 0.2 |
| [100]-oriented $MoO_3$ | 1 | 4.2 ± 0.1 |
| | 2 | 4.3 ± 0.3 |

(from 0.2 to 0.004) for the [100]-oriented $MoO_3$ crystal. These results point to: (i) a preferential activation of the oxygen molecule on the (010) face, provided the high initial labeling found in (010) and (ii) a higher oxygen mobility along the perpendicular direction to the lateral faces, namely the [100] axis, as can be derived from the relative slower decrease of the $Mo^{18}O^+$ signal arising from the [100]-oriented $MoO_3$ crystal.

Another important aspect of the process of the selective oxidation of propylene to acrolein is oxygen ion insertion into the organic intermediate chemisorbed on the catalyst surface. The extent of this process would be, in principle, evaluated by the extent of O labeling from the acrolein formed. The O labeling of $CO_2$ becomes much more difficult to interpret, since this product can be formed by direct combustion of propylene or by deep oxidation of the initially formed acrolein (*18*), the extent of this latter process being particularly important in our case owing to the large contact of the gas phase with the catalyst imposed by the closed recirculating system. Furthermore, the possibility of exchange reactions between $CO_2$ and the sample surface cannot be excluded (*19*). Consistent with this assumption, only the masses $m/e$ = 56 and 58, corresponding to oxygen-16- and oxygen-18-labeled acrolein, respectively, have been recorded. Table 1 summarizes the acrolein-18/acrolein-16 ratios obtained on the two $MoO_3$ catalyst samples analyzed by SIMS upon exposure to an $^{18}O_2 : C_3H_6$ = 2 : 1 mixture at 673 K. As can be seen this ratio does not seem to change during the reaction time. It must be pointed out that the extent of acrolein-18 labeling is almost twice as intense on [100]-oriented $MoO_3$ crystals than on (010) faces, and the proportion of acrolein-18-labeled molecules is higher than those of acrolein-16. These results are in broad agreement with those reported for graphite-supported $MoO_3$ crystals (*14*).

Finally, to learn the reactivity of oxygen vacancies, produced on the faces of $MoO_3$ crystals during heating in vacuum at 723 K, TPSR of chemisorbed NO has also been studied. This is an interesting technique, since the NO molecule usually chemisorbs on partially reduced $MoO_3$ as dimeric structures, which undergo decomposition to $N_2O$ (*20*) with the subsequent oxidation of the adsorption site upon heating. The $MoO_3$ samples used for this purpose were a [100]-oriented $MoO_3$ and a commercial $MoO_3$ powder, which exposes (010) faces and simultaneously displays a much larger surface than that of single $MoO_3$ crystals. The change of $N_2O$ partial pressure ($m/e$ = 44) produced during TPSR of adsorbed NO is shown in Fig. 5. It can be noted that practically no nitric oxide is detected in the course of TPSR. From this figure it becomes apparent that the reactivity against NO of the oxygen vacancies located in the lateral faces of $MoO_3$ ([100]-oriented $MoO_3$ sample) is higher than that present on (010) faces. On

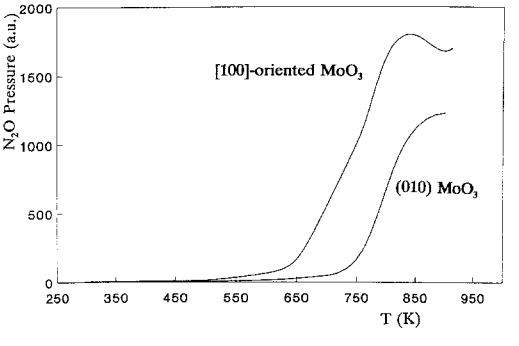


FIG. 5. TPSR of adsorbed NO followed by $N_2O$ desorption from the (010)-oriented and the [100]-oriented $MoO_3$ crystals.

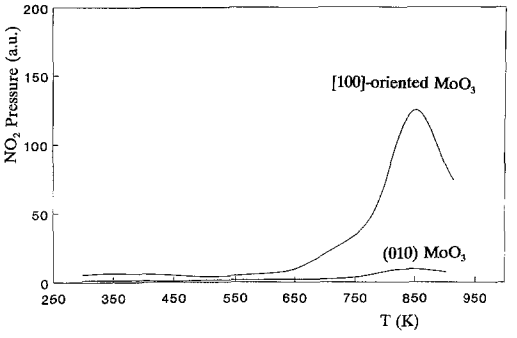


FIG. 6. TPSR of adsorbed NO followed by $NO_2$ desorption from the (010)-oriented and the [100]-oriented $MoO_3$ crystals.

the other hand, NO molecules can be oxidized by surface oxygen giving rise to $NO_2$. Figure 6 summarizes the changes of $NO_2$ ($m/e$ = 46) partial pressure brought about by TPSR of NO. It can be observed that this process occurs only to some extent in the [100]-oriented $MoO_3$ sample. Therefore, it can be concluded that the reactivity of oxygen vacancies against NO and of the surface oxygen to be incorporated into the NO is higher in the lateral faces than in the basal planes of $MoO_3$.

## DISCUSSION

As is well known, the $C_3H_6$ oxidation proceeds through several consecutive steps, the first being the $C_3H_6$ activation to allylic species, followed by the addition of oxygen ions. In mixed oxide catalysts these two steps are clearly separated; low-valent cations play the role of centers activating the olefin molecule, whereas oxygen insertion is performed by oxygen ions from the lattice of the oxides of high-valent transition metal oxides. Experimental evidence also confirms that as soon as the $C_3H_6$ molecule becomes activated to an allylic species, oxygen is rapidly inserted and the molecule of acrolein desorbed, the $C_3H_6$ activation being always the rate-determining step.

In an examination of the role of different $MoO_3$ crystal faces in elementary steps of $C_3H_6$ oxidation, Brückman *et al.* (*15*) proposed that olefin activation occurs on the (100), (001), and (101) faces, whereas the further step of lattice oxygen insertion is performed on the basal (010) face. Conversely, Volta and Tatibuet (*12*) concluded that mild oxidation to acrolein occurs on the (100) faces whereas the (010) faces are responsible for total oxidation, or even, as Guerrero-Ruíz *et al.* (*13*) suggested, both $C_3H_6$ activation and a further oxygen insertion step occur on the same face (100).

The SIMS study presented here indicates that through the pursuit of oxygen-18 within $MoO_3$ crystal, one can ascertain what sites and preferential directions for oxygen migration are involved in the selective oxidation of propylene. The SIMS data of $MoO_3$ samples used in the oxidation of propylene with oxygen-18 indicate clearly that oxygen-18 ions diffuse within the solid. It can be inferred from Fig. 4 that the dioxygen activation process takes place to a large extent in the basal planes of $MoO_3$ crystals. The oxygen-18 enrichment in the basal planes in the course of oxidation of propylene with oxygen-18 seems to be associated to the complete oxidation of propylene to $CO_2$ in that location, in good agreement with the expectation of a suprafacial phenomenon. Moreover, this suprafacial process can be interpreted as due to an easier oxygen chemisorption, and its further dissociation, on the (010) faces than on the lateral ones. On the other hand, the greater oxygen ion diffusion along the directions perpendicular to the lateral faces provides support for an intramolecular process of the selective oxidation of propylene to acrolein.

If the acrolein formation occurs on the $MoO_3$ side faces, i.e., on (100), (001), and (101) faces, the extent of oxygen-18 incorporation into the acrolein product appears surprising (Table 1). One would expect that the slow oxygen diffusion toward that face should be the same in the whole $MoO_3$ crystals. However, as already observed by other authors (*17*), the [100]-oriented $MoO_3$ samples terminate by surface planes such as (110), (120), or (130), which are closely simi-

lar and can be depicted as step surfaces composed of (100) terraces and normal (010) steps. Therefore, the results summarized in Table 1 indicating a large oxygen-18 incorporation into the [100]-oriented $MoO_3$ crystals are consistent since the activation sites in side faces and the neighboring oxygen insertion sites in the basal planes coexist in the same crystal. Moreover, these results do not provide support for the mechanism proposed by Brückman *et al.* (*15*), which assumes migration of allylic intermediates on the surface from side faces, in which propylene becomes activated, toward basal planes, in which dioxygen is activated.

As already discussed by Mingot *et al.* (*17*), the peculiar appearance of (lk0) faces, characterized for the close vicinity of Mo=O groups typical of the (010) face (where oxygen insertion could occur), and Lewis acid–base sites, typical of the (100) face (which could be active for $C_3H_6$ activation), might well explain the particular catalytic behavior of the [100]-oriented $MoO_3$ crystals. Accordingly, it appears relevent to determine the surface reactivity of $MoO_3$ crystals, which expose different faces. The major process during TPSR of NO is the reoxidation of oxygen vacancies brought about by the previous outgassing pretreatment at high temperature. The higher reactivity against NO of the [100]-oriented in respect to the (010) $MoO_3$ (Fig. 5) indicates an easier reaction pathway on the lateral faces. In favor of this conclusion note the XPS data which clearly showed the absence of reduced molybdenum species on the [100]-oriented $MoO_3$, while $Mo^{5+}$ was detected on (010) crystals. Thus, one might infer that the easier reoxidation of lateral faces by NO is associated to its selectivity for partial oxidation.

As shown in Fig. 6, the TPSR of NO revealed the appearance of the oxidation product $NO_2$ ($m/e$ = 46) in the [100]-oriented $MoO_3$, but not in the basal planes. This fact can be interpreted as due to an easier oxygen migration from the bulk toward the lateral faces of $MoO_3$, where NO begins to oxidize. This reasoning would be largely in agreement with previous TPD experiments of oxygen (*14*) and with the SIMS data shown in Fig. 4b.

In conclusion, the combined use of various kinds of experiments, including the analysis of model $MoO_3$ catalysts pretreated in propylene : oxygen-18 mixtures by SIMS depicts the general framework of the overall reaction process. It can be inferred that dioxygen is activated on the (010) basal planes and then is incorporated to the allylic species generated in the lateral faces, possessing a step-surface structure with [010] and [100] orientations. There also seems to exist a preferential migration of oxygen ions into the $MoO_3$ structure along the [100] or [001] directions.

ACKNOWLEDGMENTS

The authors acknowledge the award of Acción Integrada Hispano-Francesa 89/HF-042 (Drs. T. C. Volta and M. Abon), which has made this research possible. They further acknowledge funding of this work by CICYT, Spain, under Projects MAT 88/0239 and MAT 89/0565.

REFERENCES

1. Mars, P., and van Krevelen, D. W., *Chem. Eng. Sci., Suppl.* **3,** 41 (1954).
2. Keulks, G. W., *J. Catal.* **19,** 232 (1970).
3. Keulks, G. W., and Krenzke, L. D., *in* "Proceedings, 6th International Congress on Catalysis, London, 1976" (G. C. Bond, P. B. Wells, and F. C. Tompkins, Eds.), p. 806. The Chemical Society, London, 1976.
4. Krenzke, L. D., and Keulks, G. W., *J. Catal.* **61,** 316 (1980).
5. Keulks, G. W., Krenzke, L. D., and Notermann, T. M., *Adv. Catal.* **27,** 183 (1978).
6. Glaeser, L. C., Brazdil, F. F., Harle, M. A., Mehicic, M., and Grasselli, R. K., *J. Chem. Soc., Faraday Trans. 1* **81,** 2903 (1985).
7. Abon, M., *in* "Methodes physiques d'Etude des catalyseurs hetérogénées" (B. Imelik and J. Vedrine, Eds.), p. 474. Technipress, Paris, 1980.
8. Rodrigo, L., Adnot, A., Roberge, P. C., and Kaliaguine, S., *J. Catal.* **105,** 175 (1987).
9. Takahashi, N., Mori, T., Furuta, A., Komai, S., Miyamoto, A., Hattori, T., and Murakami, Y., *J. Catal.* **110,** 410 (1988).
10. Meijers, A. C . Q. M., deJong, A. M., van Gruijthuijsen, L. M. P., and Niemantsverdriet, J. W., *Appl. Catal.* **70,** 53 (1991).

*11.* Volta, J. C., Desquesnes, W., Moraweck, B., and Tatibuet, J. M., *in* "Proceedings, 7th International Congress on Catalysis, Tokyo, 1980" (T. Seiyama and K. Tanabe, Eds.), p. 1398. Amsterdam, 1981.

*12.* Volta, J. C., and Tatibuet, J. M., *J. Catal.* **93,** 467 (1985).

*13.* Guerrero-Ruíz, A., Abon, M., Massadier, J., and J. C. Volta, *J. Chem. Soc. Chem. Commun.,* 1031 (1987).

*14.* Guerrero-Ruíz, A., Massadier, J., Duprez, D., Abon, M., and Volta, J. C., *in* "Proceedings, 9th International Congress on Catalysis, Calgary, 1988" (M. J. Phillips and M. Ternan, Eds.), p. 1601. The Chemical Institute of Canada, 1988.

*15.* Brückman,K., Garbowski, R., Haber, J., Mazurkiewicz, A., Sloczynski, J., and Wilkowski, T., *J. Catal.* **104,** 71 (1987).

*16.* Tatibuet, J. M., Ph. D. thesis, Univ. Lyon, Lyon (1982).

*17.* Mingot, B., Floquet, N., Beltrand, O., Treilleux, M., Heizmann, J. J., Massardier, J., and Abon, M., *J. Catal.* **118,** 424 (1989).

*18.* Abon, M., Roullet M., and Guerrero-Ruíz, A., in preparation.

*19.* Patterson, W. R., *J. Mol. Catal.* **65,** L41 (1991).

*20.* Guerrero-Ruíz, A., Rodríguez-Ramos, I., Fierro, J. L. G. Fierro, Soenen, V., Herrmann, J. M., and Volta, J. C., *in* "Proceedings, 3rd European Workshop Meeting on Selective Oxidation by Heterogeneous Catalysis" (B. Delmon and P. Ruíz, Eds.), Vol. 2, p. 1. Louvain-la-Neuve, 1991.